Effect of La substitution for Gd in the ionic conductivity and oxygen dynamics of fluorite-type $Gd_2Zr_2O_7$

2007 J. Phys.: Condens. Matter 19 356212

(http://iopscience.iop.org/0953-8984/19/35/356212)

IOP PUBLISHING JOURNAL OF PHYSICS: CONDENSED MATTER

J. Phys.: Condens. Matter **19** (2007) 356212 (11pp) doi:10.1088/0953-8984/19/35/356212

Effect of La substitution for Gd in the ionic conductivity and oxygen dynamics of fluorite-type $Gd_2Zr_2O_7$

J A Díaz-Guillén[1], M R Díaz-Guillén[1], J M Almanza[1], A F Fuentes[1], J Santamaría[2] and C León[2]

[1] Cinvestav-Saltillo, Apartado Postal 663, 25000-Saltillo, Coahuila, Mexico
[2] GFMC, Departamento de Física Aplicada III, Facultad de Física, Universidad Complutense de Madrid, 28040-Madrid, Spain

Received 10 April 2007, in final form 28 June 2007
Published 8 August 2007
Online at stacks.iop.org/JPhysCM/19/356212

Abstract

We have prepared different compositions in the $Gd_{2-y}La_yZr_2O_7$ solid solution by mechanically milling stoichiometric mixtures of the corresponding oxides. Irrespective of their lanthanum content, as-prepared powder samples consist of single-phase anion-deficient fluorite materials, although the long-range ordering of cations and anion vacancies characteristic of pyrochlores was observed for $y \geqslant 0.4$ after post-milling thermal treatments at 1200 °C. Ionic conductivity was found to be thermally activated and almost independent of La content for $0 \leqslant y \leqslant 1$, since the pre-exponential factor decreases as structural ordering increases; however, there is a concomitant decrease of the activation energy E_{dc} for oxide-ion diffusion, from $E_{dc} = 1.13 \pm 0.02$ eV for the anion-deficient fluorite $Gd_2Zr_2O_7$ to $E_{dc} = 0.85 \pm 0.03$ eV for the partially ordered pyrochlore-type $Gd_{1.2}La_{0.8}Zr_2O_7$. Electrical conductivity relaxation is well described by a Kohlrausch–Williams–Watts (KWW) function of the form $\Phi = \exp(-(t/\tau)^{1-n})$, where the fractional exponent n decreases as the La content (ordering) increases. These results are explained in terms of weaker ion–ion interactions in the better ordered structure and highlight the importance of structural ordering/disordering in determining the dynamics of mobile oxygen ions.

1. Introduction

Current technology in use in solid oxide fuel cells (SOFCs) is based on a combination of a Sr-doped $LaMnO_3$ (LSM) cathode, the conventional 8YSZ solid electrolyte (yttria-stabilized zirconia with 8 mol% Y_2O_3) and a Ni-YSZ cermet anode. However, manufacturing this system requires great care since solid-state reactions between components have been frequently observed at the electrode/electrolyte interface; thus, undesirable insulating $La_2Zr_2O_7$ and

$SrZrO_3$ zirconates are formed during co-sintering or long-term operation at temperatures as low as 1000 °C. Different approaches have been suggested in the literature to overcome this problem, such as using A-site deficient LSM perovskites [1] or replacing La by some other smaller lanthanides [2]. Another possibility would consist of using the LSM cathode but a different and compatible oxide-ion conductor as the electrolyte. Amongst the additional ceramic oxides which have been examined as possible alternatives to the 8YSZ electrolyte for SOFCs with a high operating temperature, pyrochlore oxides $A_2B_2O(1)_6O(2)$, have attracted a great deal of attention because of their chemical as well as structural flexibility, including even non-stoichiometry (see [3] for a detailed description of the pyrochlore crystal structure). Electroneutrality in pyrochlore oxides can be achieved by a combination of cation species A and B, with different oxidation states; consequently their electrical properties vary from insulators or semiconductors to compounds with high ionic, electronic or mixed conductivity, which makes them suitable for the design of monolithic fuel cells [4]. Thus, while some pyrochlores such as $Gd_2Zr_2O_7$ are electronically insulating and fast high-temperature ionic conductors, others such as $Gd_2Mo_2O_7$ display a metallic conducting behavior at room temperature [3]. Interestingly, reported activation energies for oxygen migration are in general lower than those with a corresponding fluorite-type defect. Thus, a maximum in ionic conductivity and a minimum in the activation energy were found in the $Gd_yZr_{1-y}O_{2-y/2}$ solid solution for the stoichiometric pyrochlore phase P-$Gd_2Zr_2O_7$ when compared with the fluorite-type defect regions located either side in the system [5]. It has been suggested that the existence of preferential pathways for migration in the former and the associated decrease in the strain energy term of the activation energy for oxide-ion conduction, might account for these differences [6]. Furthermore, pyrochlore's intrinsic concentration of anion vacancies might be manipulated by using solid solution systems such as $Gd_2(Ti_{1-y}Zr_y)_2O_7$ between highly disordered (high Zr content) and highly ordered forms (high Ti content). Although complete order, as in the '*ideal*' pyrochlore, leads to very low conductivity values because of oxygen vacancy ordering, optimal conductivity is obtained for partially ordered phases where ionic interactions penalizing ion migration can be minimized. In this work we analyze the effect of incorporation of lanthanum on the electrical properties of $Gd_2Zr_2O_7$ and investigate compatibility of these lanthanum substituted electrolytes with LSM perovskite cathodes in solid oxide fuel cell technology.

Previous studies of pyrochlore-type oxide-ion conductors have mostly focused on the $A_2(B_{1-y}B'_y)_2O_7$ systems, with two tetravalent cations ($B, B' = Sn^{4+}, Ti^{4+}, Zr^{4+}$) simultaneously occupying the hexa-coordinated 16d site and a trivalent cation ($A = Y^{3+}$ and Ln^{3+}) on the octa-coordinated 16c site. Electrical properties in these systems are closely related to the degree of structural disorder and a large increase in ionic conductivity is observed in the $A_2(Ti_{1-y}Zr_y)_2O_7$ systems ($A = Y^{3+}$, Gd^{3+}, Dy^{3+}) with increasing disorder, that is, with increasing Zr content [7, 8]. The extent of the structural order/disorder in these solid solutions is mostly governed by the size difference between cation species occupying the A and B sites, that is, by the ionic radius ratio (R_A/R_B). When the disorder is complete this might render a fluorite-type defect structure $(A, B)_4O_7$; thus, the pyrochlore stability field at atmospheric pressure in zirconates and titanates is limited to the $1.46 \leqslant R_A/R_B \leqslant 1.78$ range. These are the ratio values calculated for $Gd_2Zr_2O_7$ and $Sm_2Ti_2O_7$, respectively, with anion-deficient fluorites obtained for $R_A/R_B < 1.46$ [3]. However, defect fluorite showing significant stability at elevated temperatures have also been prepared by mechanical milling in the $Gd_2(Ti_{1-y}Zr_y)_2O_7$ system, for compositions with R_A/R_B values well above 1.46 [9]. As for the solid solution in our present study, $Gd_{2-y}La_yZr_2O_7$, the R_A/R_B ratio value increases as the lanthanum content increases, reaching a value of 1.61 for pure $La_2Zr_2O_7$. Correspondingly, disorder enthalpies estimated using energy minimization calculations are much higher in lanthanum zirconate than

in its gadolinium analogue [10] and increasing La content should progressively drive the system towards the ordered pyrochlore crystal structure. We investigate the existence of such structural ordering as La content is increased and its possible effect on the dynamics of mobile oxygen ions and consequently on ionic conductivity values.

2. Experimental details

Several compositions with the general formula $Gd_{2-y}La_yZr_2O_7 (0 \leqslant y \leqslant 2)$ were prepared by mechanochemical synthesis. This powder processing method has already been successfully used by our group to prepare similar zirconate and titanate materials at room temperature [11, 12]. Mixtures of high-purity (>99+%) A-La_2O_3, C-Gd_2O_3 and monoclinic ZrO_2 were weighed out as required by stoichiometry and placed in 125 ml zirconia containers together with six 20 mm diameter zirconia balls (mass $\approx$ 24 g) as to keep the ball to powder mass ratio equal to 10:1. Mechanical milling was performed in air in a planetary ball mill by using a rotating disc speed of 350 rpm. Phase evolution on milling was analyzed by using x-ray powder diffraction in a Philips X'pert diffractometer using Ni-filtered Cu Kα radiation ($\lambda = 1.5418$ Å). Electrical properties were measured between 200 and 800 °C on sintered pellets (10 mm diameter and ~1 mm thickness) obtained by uniaxial pressing of the fine powders prepared by mechanical milling. To increase their mechanical strength and obtain dense samples, pellets were fired at 1200 °C for 6 h (heating and cooling rates 2 °C min^{-1}). AC impedance measurements were carried out in air by using a Solartron 1260 frequency response analyzer over the 100 Hz to 1 MHz frequency range. Electrodes were made by coating opposite faces of the pellets with conductive platinum paint and firing them at 800 °C to eliminate organic components and harden the Pt residue.

3. Results and discussion

3.1. Structural characterization

Figure 1(a) shows a comparison between the XRD patterns obtained for selected compositions after milling for 27 h as described above. The pyrochlore crystal structure might be considered as a superstructure of an anion-deficient fluorite-like atomic arrangement with twice the cell constant. Therefore, its x-ray diffraction pattern contains a set of strong reflections characteristic of the underlying fluorite-type subcell plus an additional set of reflections (i.e. the (111), (311) and (331) lines showing at ~15°, 29° and 37° (2θ), respectively), with intensities depending on factors such as the degree of ordering, the differences in the average scattering factors of the elements involved or the distribution of oxygen vacancies [13]. As figure 1(a) shows, as-prepared powder samples show XRD patterns similar to those typical of fluorites, irrespective of their La content, with no evidence of the reflections characterizing the long-range atomic ordering of the pyrochlore crystal structure being present. As a far-from-equilibrium processing method, mechanical milling allows the preparation of metastable phases and defect structures existing at equilibrium only at high temperature and/or high pressure, which are difficult to obtain or are even unattainable by any other synthetic route. Thus, powder samples prepared by mechanical milling in the solid solution, even including $La_2Zr_2O_7$, show an average crystal structure similar to that of anion-deficient fluorites despite R_A/R_B values being well above 1.46.

The increasing shift towards low angle (2θ) as the La content increases indicates a larger unit cell (R_{Gd}(VIII) = 1.053 Å versus R_{La}(VIII) = 1.16 Å [14]) and confirms the existence of a mechanically induced chemical reaction on milling. Figure 1(b) shows a comparison between

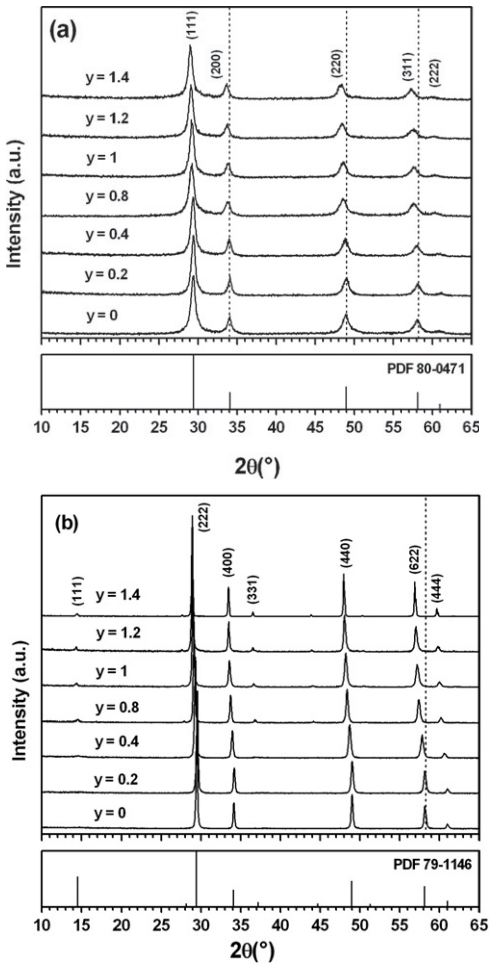

Figure 1. (a) Comparison between the XRD patterns obtained for selected compositions in the title solid solution, after milling for 27 h. As a reference, the reported XRD pattern of F-$Gd_2Zr_2O_7$ is shown at the bottom whereas numbers in parenthesis are the Miller indices of each reflection. (b) XRD patterns collected for the same powder samples after firing for 6 h at 1200 °C. Reflections characterizing the pyrochlore crystal structure are evident for at least $y \geqslant 0.4$. As a reference, the reported XRD pattern of P-$Gd_2Zr_2O_7$ is shown at the bottom. Vertical dashed lines are only shown to emphasize structural changes as the La content increases.

the XRD patterns collected for the same samples after firing for 6 h at 1200 °C. Superstructure reflections characterizing the long-range atomic ordering of the pyrochlore crystal structure, such as for example the (331) peak at ≈37° (2θ), are now evident, at least for $y \geqslant 0.4$, suggesting that a thermally driven ordering process has taken place. A similar behavior was observed in samples prepared by mechanical milling in the $Gd_2(Ti_{1-y}Zr_y)_2O_7$ system, with the temperature of the fluorite-to-pyrochlore phase transition decreasing as expected as the Ti content increases, that is, as the R_A/R_B increases. Interestingly, as-prepared $Gd_2Zr_2O_7$ and $Gd_{1.8}La_{0.2}Zr_2O_7$ powders retain the fluorite-type structure even after firing at 1200 °C.

Therefore, processing powder mixtures of ZrO_2, La_2O_3 and Gd_2O_3 in a planetary ball-mill with a moderate rotating disc speed allows the room-temperature preparation of single-phase

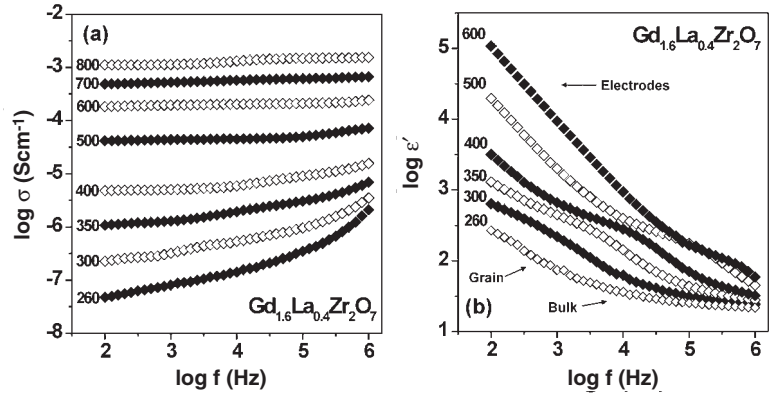

Figure 2. Frequency dependence of the real parts of (a) conductivity and (b) permittivity of $Gd_{1.6}La_{0.4}Zr_2O_7$, at selected temperatures.

$Gd_{2-y}La_yZr_2O_7$ powders. Irrespective of their La content, as-prepared metastable samples show XRD patterns similar to those characteristic of anion-deficient fluorites, and for samples with $y \geqslant 0.4$, post-milling thermal treatments facilitate the long-range ordering of the cation and anion sublattices characteristic of pyrochlores.

3.2. Electrical properties

Figure 2(a) shows the frequency and temperature dependence of the real part of the electrical conductivity, $\sigma'(\omega)$, for the as-prepared pyrochlore-type $Gd_{1.6}La_{0.4}Zr_2O_7$ sample fired for 6 h at 1200 °C, selected as representative of the series. Similar conductivity plots were obtained for all samples analyzed in this work. As this figure shows, the frequency dependence of conductivity at low temperature may be well described by the so-called Jonscher empirical expression [15], $\sigma'(\omega) \propto \omega^n$, with a fractional exponent n ($0 \leqslant n < 1$), consistent with a power law-type dependence at high frequencies and an almost frequency-independent conductivity plateau associated with the dc conductivity regime, σ_{dc}, at low frequencies. The existence of blocking effects at grain boundaries is also evident in this graph as a small decrease in the conductivity values, at low enough frequencies, thus marking the end of the conductivity plateau. At the highest temperatures (above 700 °C) blocking effects at the electrodes are also visible at the lowest frequencies. Thus, σ_{dc} at a given temperature can be directly obtained from ac conductivity measurements as the conductivity value in the plateau region of the isothermal curves in figure 2(a). The presence of the above-mentioned dispersive region has been linked to the existence of cooperative effects in the dynamics of hopping ions [16], with the fractional exponent n determined by the strength of the ion–ion interactions in the ionic hopping process; i.e. in the absence of interactions among mobile ions (completely independent and random ion hopping), the exponent n would be 0. Figure 2(b) shows the real part of the dielectric permittivity as a function of frequency for the same composition and temperatures. Again, blocking effects at grain boundaries and electrodes are observed at low frequencies with increasing temperature. The value of the high-frequency permittivity, $\varepsilon_\infty = 22 \pm 4$, is found to be almost independent of temperature and La content in the whole series.

Electrical relaxation data may also be described in terms of the electric modulus, which is the inverse of the dielectric permittivity, and thus is directly related to the conductivity through

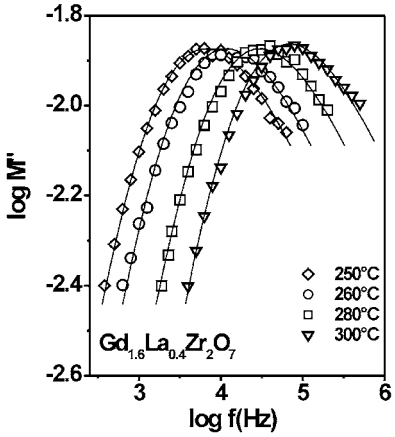

Figure 3. Frequency dependence of the imaginary part of the electric modulus for $Gd_{1.6}La_{0.4}Zr_2O_7$, at different temperatures. Solid lines are best fits to peak maxima according to a KWW relaxation function.

the equation:

$$M^*(\omega) = 1/\varepsilon^*(\omega) = \mathrm{j}\omega\varepsilon_0/\sigma^*(\omega). \tag{1}$$

The electric modulus can then be expressed by the Fourier transform of the time derivative [17, 18]

$$M^*(\omega) = \frac{1}{\varepsilon_\infty}\left[1 - \int_0^\infty \left(-\frac{\mathrm{d}\Phi}{\mathrm{d}t}\right)\mathrm{e}^{-\mathrm{j}\omega t}\,\mathrm{d}t\right] \tag{2}$$

of the so-called Kohlrausch–Williams–Watts (KWW) relaxation function of the form [18, 19]

$$\Phi(t) = \exp(-(t/\tau)^{1-n}), \qquad 0 < (1-n) \leqslant 1 \tag{3}$$

where ε_∞ is the dielectric permittivity at high frequencies and τ the characteristic relaxation time of the ion-hopping process which is thermally activated with the same activation energy as the dc conductivity. Correspondingly, the time dependence indicated in equation (3) is reflected by the spectral shape of the imaginary part of the electric modulus as an asymmetric relaxation peak at a characteristic frequency $\omega_\mathrm{p} \approx \tau^{-1}$, which increases with increasing temperature. The fractional exponent n defines the power law dependence of $M''(\omega)$ above the peak frequency as ω^{n-1}, and consequently the power law dependence of the real part of the conductivity ($\sigma'(\omega) \approx \omega^n$) at high frequencies. Thus, the value of n is a measure of the departure from the pure exponential or Debye behavior expected for uncorrelated ion hopping. Figure 3 shows the frequency dependence of the imaginary part of the electric modulus at three selected temperatures for the same $Gd_{1.6}La_{0.4}Zr_2O_7$ powder sample. The figure also shows best fits according to equations (2) and (3), in excellent agreement with experimental data, and from which the values of the exponent n are obtained and observed to be temperature independent for each sample.

As $La_2Zr_2O_7$ has been shown to be a mixed p-type and ionic conductor at high temperature [20], we have limited our analysis of oxygen dynamics in the series to samples with $y \leqslant 1.2$ where the electronic contribution is negligible and dc conductivity is purely ionic. The value of the exponent n was found to decrease with increasing lanthanum content from 0.52 ± 0.01 for $Gd_2Zr_2O_7$ to 0.46 ± 0.01 for $Gd_{0.8}La_{1.2}Zr_2O_7$. This is consistent with the previous finding that the exponent n is related to the degree of structural order/disorder

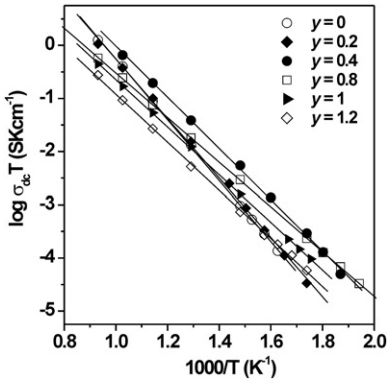

Figure 4. Arrhenius-type plots for selected compositions in the $Gd_{2-y}La_yZr_2O_7$ solid solution.

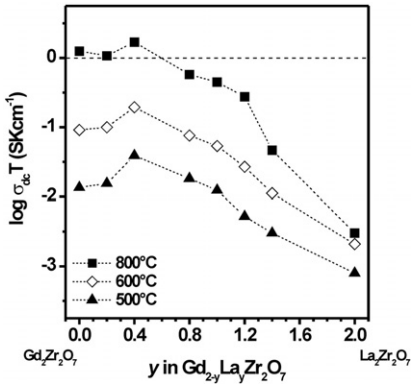

Figure 5. dc conductivity versus La content for the $Gd_{2-y}La_yZr_2O_7$ solid solution at three selected temperatures.

in ionically conducting pyrochlore oxides [21]. In the present case, a more ordered structure is induced by increasing lanthanum content as found in the structural characterization, and n decreases accordingly.

Figure 4 presents Arrhenius plots showing the temperature dependence of the dc conductivity for selected compositions sintered at 1200 °C. All samples show a thermally activated behavior of the form $\sigma_{dc} \cdot T = (\sigma_0) \exp(-E_{dc}/k_B T)$, where σ_0 is the pre-exponential factor which is related to the effective number of mobile oxygen ions and E_{dc} denotes the activation energy for the ion conduction process.

Activation energy values for dc conductivity, E_{dc}, obtained from the slope of these plots were found to decrease significantly with increasing lanthanum content, from 1.13 ± 0.02 eV for the highly disordered anion deficient fluorite $Gd_2Zr_2O_7$ ($\sigma_0 = 2.9 \times 10^5$) to 0.85 ± 0.03 eV for partially ordered pyrochlore-type compositions with $0.8 \leqslant y \leqslant 1.2$ ($\sigma_0 = 6.8 \times 10^3$). Simultaneously, the dc conductivity for the series (see figure 5) shows a maximum for $y = 0.4$ at low temperatures whereas it is almost independent of La content above 500 °C. As the XRD patterns revealed (figure 1(b)), $Gd_{1.6}La_{0.4}Zr_2O_7$ turns out to be the first composition in which the pyrochlore superstructure reflections become evident. Therefore, the onset of long-range ordering of cations and anion vacancies characteristic of pyrochlores is linked to a conductivity maximum, in good agreement with previous observations in the Ln_2O_3–ZrO_2 system [5, 6].

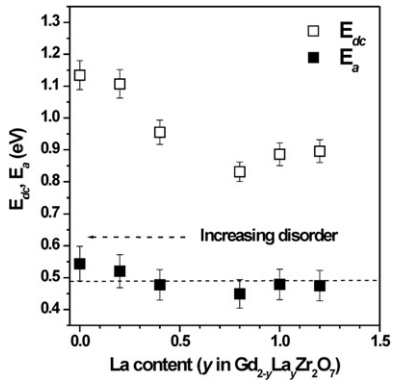

Figure 6. Values obtained for the activation energy E_{dc} (□) and the energy barrier $E_a = (1 - n)E_{dc}$ (■) as a function of lanthanum content. The dashed line represents the average E_a value.

What do we know about oxygen migration in pyrochlores? Oxygen ions in 'ideal' or 'ordered' pyrochlores fully occupy two crystallographically different sites, 48f and 8a according to Wyckoff notation, leaving another possible position, 8b, systematically empty. Therefore, vacancies must be created by disordering the anion sublattice before migration can take place with the three anion positions, 48f, 8a and 8b, ending up partially occupied in 'defect' or 'disordered' pyrochlores. By using computing simulation techniques, van Dijk *et al* [22] predicted a defect structure for pyrochlores consisting of 'split vacancies', a 48f vacancy pair in the ⟨110⟩ direction with an interstitial ion in between, a scenario slightly more stable than a single 48f vacancy. A diffusion mechanism consisting of sequential jumps of oxygen atoms along the 48f sites, either between (i) nearest neighbor sites (along ⟨100⟩) and/or (ii) along ⟨110⟩ involving the 'split vacancy' structure (next nearest neighbor), was proposed to be responsible for the migration of vacancies. It has been also suggested that the 'split vacancy' configuration enhances ionic conductivity by providing greater geometrical flexibility and longer effective jump distances, becoming more stable with respect to the 48f single vacancy as disorder increases, i.e. $R_A/R_B \sim 1.46$ [23]. However, according to atomistic simulations, oxygens in 8a also play an important role in vacancy migration by providing low-energy mechanisms for diffusion at low disorder [24]. Despite the oxygen ions in 48f being coordinated by two B^{4+} and two A^{3+} cations, it has been suggested that activation energies for migration should be more dependent on the B^{4+} cation radii than on the A^{3+} size. Thus, according to [23], intermediate to large B^{4+} cations should give the lowest E_{dc}, whereas intermediate size lanthanides (Sm to Er) in the A^{3+} position would render lower activation energies than the larger trivalent elements (La to Nd). Taking all this into account, we will now discuss the observed relationship between structural order and ionic conductivity in terms of cooperative effects among mobile oxygen vacancies.

Different models have been proposed to analyze electrical relaxation data in ionic conductors [16, 25, 26] which take into account the existence of cooperative effects among mobile ions in the diffusion process. Interestingly, our results of a concomitant decrease of the activation energy E_{dc} for the dc conductivity (see figure 6) and of the value of n, with decreasing disorder, can be rationalized in terms of the coupling model (CM) [16, 25, 27, 28]. The CM starts with the consideration of independent hops of ions to vacant adjacent sites with exponential correlation function, $\Phi(t) = \exp(-t/\tau_o)$, and relaxation time τ_0. Such independent hops cannot occur for all ions at the same time because of ion–ion interactions and correlations. The result of ion–ion interactions is the slowing down of the relaxation rate

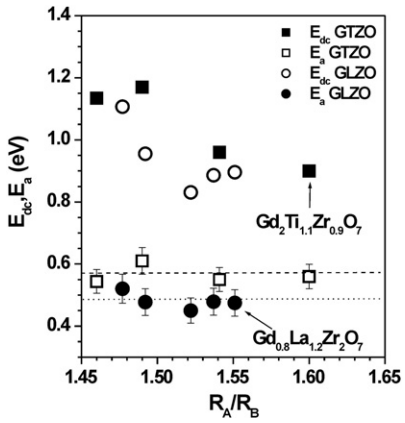

Figure 7. Activation energies E_{dc} (squares) and E_a (circles) as a function of the R_A/R_B ratio for the $Gd_{2-y}La_yZr_2O_7$ (GLZO, empty symbols) and $Gd_2(Ti_{1-y}Zr_y)_2O_7$ (GTZO, solid symbols) solid solutions. Dashed and dotted lines represent the average E_a values found for each series. All samples were prepared by mechanical milling and sintered at 1200 °C.

at times longer than t_c of the order of 2 ps, changing the correlation function from a pure exponential to a KWW function, $\Phi(t) = \exp(-(t/\tau)^{1-n})$, wherein the value of the fractional exponent n is a measure of the cooperative effects. A major result from the CM is that the effective relaxation time τ is related to τ_0 by

$$\tau = [t_c^{-n}\tau_o]^{1/(1-n)}. \tag{4}$$

For ions vibrating in their cages and hopping to neighboring sites through barriers of energy E_a, the relaxation time for independent ion hopping is $\tau_o(T) = \tau_\infty \exp(E_a/kT)$. The reciprocal of τ_∞ is the attempt frequency of ions. It follows from equation (4) that the activation energy for the dc conductivity or τ will be larger than the energy barrier and is given by the relation

$$E_{dc} = E_a/(1-n). \tag{5}$$

The increase in ion–ion interaction leads to a higher degree of cooperativity in the ion hopping process which corresponds to a higher value of n and, consequently, to higher activation energy for long-range ionic transport due to the energy penalty that ion–ion interactions impose on the ionic diffusion process. In fact, the activation energy E_a for the barrier that oxygen ions must overcome to hop (independently) between neighboring vacant sites in the $Gd_{2-y}La_yZr_2O_7$ series ($0 \leqslant y \leqslant 1.2$), can thus be estimated according to equation (5) by using the experimental values obtained for E_{dc} and n. A value $E_a = 0.49 \pm 0.04$ eV is found, independent of La content within experimental error (figure 6).

As deduced from the XRD data, a lower La content leads to a higher degree of structural disorder, where enhanced ion–ion interactions are expected, and consequently also to higher values of the exponent n according to the CM. The more disordered structure fosters ion–ion correlations, and leads to an increase of the energy penalty that these correlations impose on long-range or dc ionic conductivity. This explains the larger difference found between E_{dc} and E_a (larger value of n), the lower the La content for the $Gd_{2-y}La_yZr_2O_7$ series (see figure 6).

It is of interest to compare these results with those obtained by ourselves in powder samples with different Ti/Zr ratio values in the better known $Gd_2(Ti_{1-y}Zr_y)_2O_7$ solid solution, also prepared by mechanical milling and fired at 1200 °C. As figure 7 shows, and for similar values of the R_A/R_B ionic radius ratio, La substitution for Gd renders lower activation energies E_{dc} and E_a than that of Zr for Ti (average E_a values are 0.49 ± 0.04 eV versus 0.57 ± 0.03 eV,

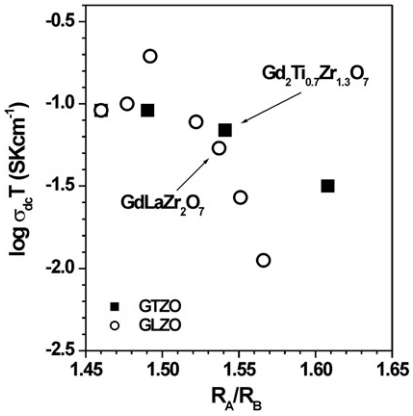

Figure 8. dc conductivity values measured at 500 °C for both solid solutions $Gd_{2-y}La_yZr_2O_7$ (GLZO, circles) and $Gd_2(Ti_{1-y}Zr_y)_2O_7$ (GTZO, squares) as a function of the R_A/R_B ratio.

respectively). Correspondingly, as one can see in figure 8, both solid solutions have similar dc conductivity values at 500 °C (at least for La substitution for Gd up to 50%). These results suggest that the A cations also play an important role in determining the energy penalty for migration and therefore that the use of mixed lanthanide solid solutions might be an interesting strategy to achieve lower activation energies for oxide-ion conductivity in pyrochlores. Finally, it is worthwhile noting that atomistic simulations in the $Gd_2(Ti_{1-y}Zr_y)_2O_7$ solid solution [24] have predicted activation energies close to 0.6 eV for the diffusion mechanism through the 48f to 48f path, in good agreement with our estimations for E_a, giving further support to our findings.

4. Conclusions

We have shown that compositions in the $Gd_{2-y}La_yZr_2O_7$ solid solution having different Gd/La ratios can be easily prepared at room temperature by mechanically milling stoichiometric mixtures of the corresponding elemental oxides. As-prepared powder samples show XRD patterns similar to those characteristic of highly disordered anion-deficient fluorites, while post-milling thermal treatments at 1200 °C give rise to a partial redistribution of cations and oxygen vacancies and the appearance of the long-range atomic ordering characteristic of pyrochlores for $y \geqslant 0.4$. Accordingly, activation energy for migration decreases as ordering increases (La content) and dc conductivity in the series reaches a maximum for $y = 0.4$ at low temperatures ($\leqslant$500 °C) whereas at high temperatures it is almost independent of La content for $y \leqslant 1$. From the analysis of electrical conductivity relaxation in terms of Ngai's coupling model we conclude that this behavior is due to the weakening of ion–ion interactions promoted by the more ordered structure in samples with higher La content. Interestingly, the $Gd_{2-y}La_yZr_2O_7$ series show high oxide-ion conductivity values for $y \leqslant 1$, similar to those measured in the better known $Gd_2(Ti_{1-y}Zr_y)_2O_7$ solid solution, as a consequence of the lower activation energies for ionic conduction.

Acknowledgments

This work has been carried out with the financial support of Mexican Conacyt (Grant SEP-2003-C02-44075) and Spanish MCYT (MAT2004-3070-C05).

References

[1] Yokokawa H, Sakai N, Kawada T and Dokiya M 1991 *J. Electrochem. Soc.* **138** 2719–27
[2] Takeda Y, Sakaki Y, Tu H-Y, Phillipps M B, Imanishi N and Yamamoto O 2000 *Electrochemistry* **68** 764–70
[3] Subramanian M, Aravamudan G and Subba Rao G V 1983 *Prog. Solid State Chem.* **15** 55–143
[4] Tuller H L 1996 *Proc. 17th Riso Int. Symp. on Materials Science* ed F Poulsen, N Bonanos, S Linderoth, M Mogensen and B Zachau-Chistiansen (Roskilde: Riso National Laboratory) pp 139–53
[5] van Dijk T, de Vries K J and Burggraaf A J 1980 *Phys. Status Solidi* **58** 115–25
[6] Burggraaf A J, van Dijk T and Verkerk M J 1981 *Solid State Ion.* **5** 519–22
[7] Moon P K and Tuller H L 1989 *Solid State Ionics; Mater. Res. Soc. Proc.* vol 135, ed G Nazri, R A Huggins and D F Shriver, pp 149–63
[8] Moreno K J, Guevara-Liceaga M A, Fuentes A F, García-Barriocanal J, León C and Santamaría J 2006 *J. Solid State Chem.* **179** 928–34
[9] Moreno K J, Fuentes A F, Maczka M, Hanuza J and Amador U 2006 *J. Solid State Chem.* **179** 3805–13
[10] Minervini L, Grimes R W and Sickafus K E 2000 *J. Am. Ceram. Soc.* **83** 1873–8
[11] Moreno K J, Silva Rodrigo R and Fuentes A F 2005 *J. Alloys Compounds* **350** 230–5
[12] Fuentes A F, Boulahya K, Maczka M, Hanuza J and Amador U 2005 *Solid State Sci.* **7** 343–53
[13] Heremans C, Wuensch B J, Stalick J K and Prince E 1995 *J. Solid State Chem.* **117** 108–21
[14] Shannon R D 1976 *Acta Crystallogr.* A **32** 751–67
[15] Jonscher A K 1984 *Dielectric Relaxation in Solids* (London: Chelsea Dielectric Press)
[16] Ngai K L and Rendell R W 1997 *ACS Symposium Series* vol 676, pp 45–66
[17] Ngai K L and León C 1999 *Phys. Rev.* B **60** 9396–405
[18] Macedo P B, Moynihan C T and Bose R 1972 *Phys. Chem. Glasses* **13** 171–9
[19] Kohlrausch R 1847 *Pogg Ann. Phys.* **72** 353
[20] Etsell T H and Flengas S N 1970 *Chem. Rev.* **70** 339–76
[21] Moreno K J, Mendoza-Suárez G, Fuentes A F, García-Barriocanal J, León C and Santamaría J 2005 *Phys. Rev.* B **71** 132301
[22] van Dijk M P, Burggraaf A J, Cormack A N and Catlow C R A 1985 *Solid State Ion.* **17** 159–67
[23] Pirzada M, Grimes R W, Minervini L, Maguire J F and Sickafus K E 2001 *Solid State Ion.* **140** 201–8
[24] Williford R E, Weber W J, Devanathan R and Gale J D 1999 *J. Electroceram.* **3** 409–24
[25] Ngai K L and León C 1999 *Solid State Ion.* **125** 81–90
[26] Funke K, Banhatti R D and Cramer C 2005 *Phys. Chem. Chem. Phys.* **7** 157–65
[27] Ngai K L and León C 2002 *Phys. Rev.* B **66** 064308
[28] Ngai K L and León C 2003 *J. Non-Cryst. Solids* **315** 124–33